CrystEngComm

ROYAL SOCIETY OF CHEMISTRY

PAPER

View Article Online
View Journal | View Issue

Cite this: *CrystEngComm*, 2025, **27**, 7884

Chloro-containing host compounds with fused tricyclic moieties and diamino linkers: host ability and affinity behaviour in pyridine/methylpyridines

Danica B. Trollip, *[a] Benita Barton, *[a] Mino R. Caira *[b] and Eric C. Hosten [a]

N,*N*′-Bis(9-(4-chlorophenyl)-9-thioxanthenyl)ethylenediamine (**H1**) and *N*,*N*′-bis(9-(4-chlorophenyl)-9-xanthenyl)ethylenediamine (**H2**) were investigated as possible separation agents for mixtures of pyridine (PYR) and methylpyridine isomers (2MP, 3MP, and 4MP) through supramolecular chemistry. MPs are present as mixtures in the chemical industry, but fractional distillation is challenging since they have a narrow boiling range, and so alternative and greener separation strategies are necessary. Initially, the host ability of **H1** and **H2** was assessed for these solvents; each pyridine was enclathrated by both host compounds. When guests competed, **H1** and **H2** behaved selectively: host affinities were in the order 3MP > PYR > 4MP ≫ 2MP (**H1**) and 2MP > 3MP > PYR ≫ 4MP (**H2**). Moreover, **H1** was able to separate the 80 : 20, 60 : 40 and 50 : 50 PYR/2MP, 20 : 80 3MP/PYR and 60 : 40 PYR/4MP mixtures: high selectivity coefficients were calculated ($K \geq 10$). **H2** fared even better: each of the 20 : 80 2MP/PYR, 40 : 60 and 20 : 80 3MP/PYR, all mixtures of PYR/4MP except 20 : 80, all solutions of 2MP/4MP and 20 : 80 3MP/4MP mixtures may be purified in this fashion. Thermal experiments demonstrated that the favoured guest solvents formed the more stable complexes with **H1** and **H2**. Furthermore, the SCXRD analyses provided reasons for the host affinity of **H1** for 3MP, relative to the least preferred 2MP, when presented with guest mixtures. 3MP experienced three C–H···π close contacts with the host molecule, while this type of interaction was not observed in the 2MP-containing complex. Finally, 4MP was consistently disfavoured by **H2** as a result of the fact that this guest solvent was accommodated in wide open multidirectional channels and, as a result, was the least stable complex, confirmed by thermal analysis, while the favoured 2MP formed the most stable complex of the four, being housed in unidirectional channels.

Received 9th October 2025,
Accepted 3rd November 2025

DOI: 10.1039/d5ce00969c

rsc.li/crystengcomm

1. Introduction

Pyridine (PYR) and its methylpyridine positional isomers (2MP, 3MP and 4MP) were traditionally obtained from the heating of coal in ovens to produce coke.[1] Subsequent to that, many methods for the synthesis of these pyridines have been reported owing to the increasing demand for these aromatic organic heterocycles. Most notable is the method of Chichibabin,[2–4] which involves condensing aldehydes, ketones and/or α,β-unsaturated carbonyl compounds with ammonia. More specifically, 2MP and 4MP are produced as a mixture when acetaldehyde and ammonia condense, while PYR and 3MP are the result when the reagents are acrolein and ammonia.[5] These syntheses are carried out at high temperatures, 350–500 °C, and are more effective in the presence of catalysts such as silicon dioxide or alumina.

Since such synthetic procedures usually result in mixed pyridines, as indicated above, subsequent separations are required in order to isolate each one since they typically have their own dedicated applications in the chemical industry. A few examples follow. Unsubstituted pyridine serves as an excellent solvent in many processes since it dissolves in both water and many organic liquids and is also required for the synthesis of active pharmaceutical ingredients (APIs) and agrochemicals.[6–8] 2MP serves also as an intermediate towards APIs,[5] and many of its reactions centre around the 2-methyl moiety. For instance, 2MP is required for the preparation of 2-vinylpyridine which is a necessary monomer when preparing textile tire cord. The same is true for 3MP, which is ultimately converted to pyridine-3-carbaldehyde, an intermediate towards antidotes for various poisons.[9–12] The 4-methyl isomer, similarly, is a building block for the formation of many medicinal compounds, an example being isonicotinic acid which is required for the preparation of anti-tubercular APIs.

[a] *Department of Chemistry, Nelson Mandela University, PO Box 77000, Gqeberha (Port Elizabeth), 6031, South Africa. E-mail: s217468225@mandela.ac.za, benita.barton@mandela.ac.za*
[b] *Department of Chemistry, University of Cape Town, Rondebosch 7701, South Africa. E-mail: mino.caira@uct.ac.za*

While PYR has a different boiling point (115.2 °C) compared with its methyl-substituted analogues and may thus be separated from these isomers by means of fractional distillation, the boiling points of the MPs are comparable (128–129, 144 and 145 °C for 2MP, 3MP and 4MP),[13] rendering this separatory technique extremely energy intensive, costly, cumbersome and, ultimately, ineffective.[14,15] Consequently, alternative separation methodologies are essential. To this end, the scientific literature abounds with reports proposing other more efficient methods for such separations. It has been reported that, for example, PYR and 3MP may be separated completely from one another by means of the macrocyclic host compound, cucurbit[6]uril.[16] Other methods of separation include the employment of metal–organic frameworks (MOFs), calixarene derivatives, capillary zone electrophoresis and chromatography.[17–20]

Host–guest chemistry involving the encapsulation of guest species within the permanent voids of large macrocyclic host molecules or in the transient intrinsic cavities characterised by relatively small host molecules has received much attention in the last few years owing to its wide variety of useful applications. These include, but are not limited to, energy and chemical storage, chemosensing, water purification, stability and delivery of APIs, and racemate resolution.[21–27]

In the present investigation, we have considered two molecules, namely *N*,*N*′-bis(9-(4-chlorophenyl)-9-thioxanthenyl)ethylenediamine (**H1**) and *N*,*N*′-bis(9-(4-chlorophenyl)-9-xanthenyl)ethylenediamine (**H2**), for, firstly, their host ability for these pyridines (Scheme 1) and, secondly, their possible separation of mixtures of these guest solvents through host–guest chemistry as an alternative and greener methodology relative to fractional distillation. If host ability exists, these compounds may even be considered later for the purification of fouled water since these pyridine solvents are frequently found in wastewater.[28–30] Any successfully prepared inclusion compounds here were subjected to SCXRD analyses to assess how the guest molecules were captured within the crystals of their complexes as well as thermoanalytical experiments as a means of establishing their relative thermal stabilities. We report on these findings now.

2. Methods

2.1 General

All chemicals pertinent to the present investigation were purchased from Merck (South Africa) and were used without further modification.

2.2 ^{1}H-NMR spectroscopy

^{1}H-NMR experiments were carried out by means of a Bruker Ultrashield Plus 400 MHz spectrometer. Resultant data were analysed using Topspin 4.2, while $CDCl_3$ served as the deuterated solvent.

2.3 Thermal analyses

These experiments were performed on all single solvent complexes synthesized in this work. A Perkin Elmer STA6000 simultaneous thermal analyser was the applicable instrument and high purity nitrogen was the purge gas. The crystals were first isolated from their solutions by means of vacuum filtration and washed, also under vacuum, with petroleum ether (bp 40–60 °C), and then patted dry in folded filter paper. The solids were then placed in a ceramic pan (which served earlier also as the reference) and heated from approximately 40 to 340 °C; the heating rate was 10 °C min^{-1}. The data thus captured were analysed by means of Perkin Elmer Pyris 13 thermal analysis software.

2.4 Gas chromatography

The quantification of the pyridines in the mixed guest complexes required gas chromatographic analysis. An Agilent J&W Cyclosil-B column served as the stationary phase, while the applicable instrument was either an Agilent 7890A or a Young Lin YL6500 GC. High purity nitrogen or helium served as the carrier gas, and the method involved an initial 5 min hold time at 50 °C, followed by a heating ramp of 5 °C min^{-1} until 100 °C was reached. In each experiment, the split ratio was 1 : 80.

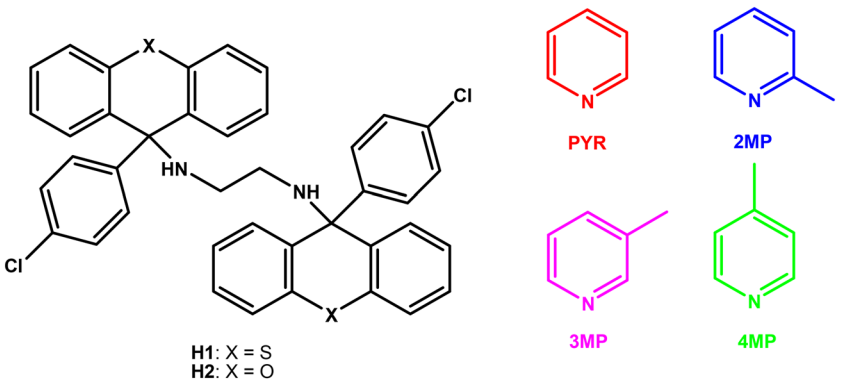

Scheme 1 The molecular structures of **H1**, **H2** and the potential guest solvents PYR, 2MP, 3MP and 4MP.

2.5 SCXRD experiments

These analyses were carried out by means of two diffractometers, the first being a Bruker Kappa APEXII diffractometer with graphite-monochromated MoKα radiation (λ = 0.71073 Å). APEXII was used for data collection, and unit cell refinement and data reduction were carried out by means of SAINT.[31] The structures were solved with SHELXT-2018/2,[32] and refinement required the least-squares procedures in SHELXL-2018/3 (ref. 33) and SHELXLE[34] (as a graphical interface (GUI)). Carbon-bound hydrogen atoms were added in idealized geometrical positions in a riding model and all non-hydrogen atoms were refined anisotropically. Data were corrected for absorption effects with the numerical method in SADABS.[33] The second instrument was a Bruker D8 VENTURE diffractometer also with graphite-monochromated MoKα radiation. The crystal was cooled to 100(2) K with nitrogen vapour from a cryostream (Oxford Cryosystems). Data collection was performed with ω- and ϕ-scans of width 1.0° and was controlled using APEX3/v2019.1-0 (Bruker) software; refinement of the unit cell and data reduction were carried out by means of the program SAINT v8.40A (Bruker).[35] Absorption corrections were applied using the multi-scan method with SADABS (2016/2).[36] The structures were solved by direct methods and refined by full-matrix least-squares (programs in the SHELX suite).[37] As a GUI, version 4.0 of X-Seed (a program for supramolecular crystallography) was applicable.[38] In the final cycles of refinement, all non-hydrogen atoms were treated anisotropically, while hydrogen atoms were added in idealized positions in a riding model after their unequivocal location in successive difference Fourier maps. Finally, the eight crystal structures were deposited at the Cambridge Crystallographic Data Centre (CCDC) and their corresponding CCDC numbers are provided in Tables 5 and 6.

2.6 Preparation of the two host compounds H1 and H2

The two host compounds **H1** and **H2** were synthesized after a consideration of previous reports.[39–44]

2.7 Single solvent host crystallization experiments

At the outset, the host ability of **H1** and **H2** was established by means of crystallization experiments from each of the pyridyl guest solvents. Therefore, in a glass vial was dissolved the host compound (0.03 g) in the guest solvent (5 mmol). Mild heat was applied to ensure that all of the host compound dissolved, where necessary. The vials were left open to the atmospheric temperature and pressure, which facilitated the slow evaporation of some of the guest solvent from the solution, ultimately resulting in crystallization. The crystals were collected through suction filtration, washed with petroleum ether (bp 40–60 °C) while still under suction, and then analysed by means of ^{1}H-NMR spectroscopy. The presence of guest resonance signals in the resultant NMR spectrum confirmed the formation of a complex in this manner, and the host : guest (H : G) ratio was calculated by comparing the areas of suitable host and guest resonance signals.

2.8 Host crystallization experiments from equimolar mixed guest solutions

The selectivity behaviour of both host compounds was subsequently investigated. This was readily achieved by mixing the pyridyl guest solvents (all possible combinations were considered, *i.e.*, binary, ternary and quaternary mixtures) in equimolar proportions and then crystallizing each host compound from this solution. Hence, 0.03 g of the host species was dissolved in a 5.00 mmol combined amount of each guest solution. Vials were closed and stored at a low temperature (4 °C, to minimize guest evaporation and maintain equimolar conditions). The resulting crystals under these conditions were treated as in the single guest solvent experiments. Analyses involved both ^{1}H-NMR spectroscopy to determine overall H : G ratios and GC for quantification purposes of the guests in the mixed guest complexes.

2.9 Binary non-equimolar mixed guest experiments

By considering the equation of Pivovar and coworkers (eqn (1)),[45] the selectivity behaviour of each host compound was assessed and measured when crystallized from binary mixed guest solutions, where the molar amounts of guest A (G_A) and guest B (G_B) were varied to 20 : 80, 40 : 60, 60 : 40 and 80 : 20 (note that the 50 : 50 G_A : G_B results from the earlier binary equimolar experiments were also considered here). The treatment of the vials in which these experiments were conducted and the analysis of the ensuing solids were as in the equimolar experiments.

$$K = \frac{Z_A}{Z_B} \times \frac{X_B}{X_A} \quad (1)$$

where $X_A + X_B = 100$, $Z_A + Z_B = 100$ and K is the selectivity coefficient, which describes the selectivity behaviour of the host compound under these conditions. $K = 1$ represents a host compound that is not selective.

It was then possible to construct selectivity profiles in a visual manner to observe the host selectivity behaviour. This was achieved by plotting Z_A (or Z_B), the amount of G_A (or G_B) in the crystals, against X_A (or X_B), the amount of the same guest in the original solution. The $K = 1$ event is represented by means of the straight diagonal lines in these diagrams; any data points obtained experimentally that deviate from this line indicate that the host compound indeed exhibited selectivity for one of the two guest species present. It has been reported that a K value of 10 or greater implies that these separations are possible industrially,[46] and so the K value for each experimentally obtained data point was calculated in this part of the investigation in order to determine which binary solutions may be separated in this manner.

Table 1 The H : G ratios obtained after host crystallization experiments from the pyridyl solvents[a]

Guest	H1	H2
PYR	1 : 1	1 : 2
2MP	2 : 1	1 : 2
3MP	1 : 1	1 : 2
4MP	2 : 1	2 : 3

[a] The H : G ratios were determined by means of ^{1}H-NMR spectroscopy.

2.10 Software

The program Mercury version 2024.3.1[47] was used in order to observe the host–guest packing, the unit cells and the nature of the voids that accommodated the guest molecules. In order to illustrate the guest accommodation, each guest species was deleted from the packing calculations, which resulted in the formation of spaces in the structure. These were explored by means of a probe with a radius of 1.2 Å to obtain the void diagrams presented in this work. Mercury was also employed to investigate the noncovalent close contacts in these complexes that were responsible for guest retention in the crystals of the complex and for maintaining the host–guest packing motif.

3. Results and discussion

3.1 Single solvent host crystallization experiments

After crystallizing **H1** and **H2** from each of the guest solvents and analysing the resultant solids using ^{1}H-NMR spectroscopy, Table 1 was populated with the calculated H : G ratios (all applicable ^{1}H-NMR spectra are deposited in the SI).

In this manner, inclusion complexes were formed in each instance; **H1** included PYR, 2MP, 3MP and 4MP with H : G ratios of 1 : 1, 2 : 1, 1 : 1 and 2 : 1, respectively, while these ratios were 1 : 2, 1 : 2, 1 : 2 and 2 : 3 in the case of **H2** (Table 1).

3.2 Host crystallization experiments from equimolar mixed guest solutions

The equimolar mixed pyridyl experiments furnished the results as provided in Table 2 after GC analysis (to quantify the guests in the mixed guest complexes) and ^{1}H-NMR experiments (for the overall H : G ratios) on the solids that were isolated from each solution. Preferred guests are highlighted in bold text. These experiments were conducted in duplicate and so the percentage estimated standard deviations (% e.s.d.s) are provided in parentheses in this table (the GC traces may be found in the SI).

For host compound **H1**, when crystallized from the equimolar binary guest mixtures, a preference towards 3MP was consistently observed, and the crystals from these experiments contained as much as 72.0–83.3% 3MP (Table 2). In the absence of 3MP, PYR and then 4MP were favoured. An extraordinary result was observed in the PYR/2MP experiment, where as much as 93.0% PYR was measured in the crystals. In the ternary mixtures, 3MP remained the preferred guest solvent, and the greatest percentage of 3MP in these cases was noted in the PYR/2MP/3MP experiment (71.3%). In PYR/2MP/4MP, where 3MP was not present, the host selectivity was then for PYR once more (77.6%). Finally, and interestingly, the quaternary guest solvent experiment demonstrated that **H1** now favoured, overwhelmingly, PYR (54.3%) rather than 3MP (13.0%), contrary to expectations given the results from the other equimolar experiments reported in this table.

In summary, the selectivity of **H1** was generally in the order 3MP > PYR > 4MP ≫ 2MP, with 2MP consistently being disfavoured in these experiments.

Contrastingly, the host affinity of **H2** was towards 2MP in the binary guest mixtures (Table 2), with a significant selectivity observed for this guest solvent in the 2MP/4MP experiment (91.9%). When 2MP was absent from the binary mixtures, then more of 3MP was selected (the PYR/3MP and 3MP/4MP experiments afforded complexes with 61.7 and 75.1% 3MP, respectively) followed by PYR. In fact, the PYR/

Table 2 Results from the equimolar mixed guest competition experiments

Guests				Guest ratios (% e.s.d.s)		Overall H : G ratio	
PYR	2MP	3MP	4MP	**H1**	**H2**	**H1**	**H2**
X	X			**93.0** : 7.0 (1.0)	26.1 : **73.9** (0.8)	4 : 3	1 : 3
X		X		17.3 : **82.7** (2.0)	38.3 : **61.7** (2.3)	2 : 3	1 : 2
X			X	**74.7** : 25.3 (2.3)	**96.2** : 4.8 (1.9)	1 : 1	1 : 2
	X	X		16.7 : **83.3** (2.5)	**69.7** : 30.3 (0.6)	2 : 3	2 : 5
	X		X	26.0 : **74.0** (0.7)	**91.9** : 8.1 (0.8)	3 : 2	2 : 5
		X	X	**72.0** : 28.0 (4.4)	**75.1** : 24.9 (0.4)	1 : 1	1 : 3
X	X	X		15.7 : 13.0 : **71.3** (0.9)(1.1)(0.3)	19.8 : **60.6** : 19.6 (0.4)(1.7)(1.3)	1 : 2	2 : 5
X	X		X	**77.6** : 12.6 : 9.8 (0.3)(2.1)(1.8)	27.3 : **67.9** : 4.8 (2.0)(0.7)(1.3)	1 : 1	1 : 3
X		X	X	15.4 : **55.6** : 29.0 (1.3)(1.0)(2.3)	26.9 : **60.1** : 13.0 (0.3)(0.8)(0.5)	1 : 1	1 : 3
	X	X	X	13.5 : **69.6** : 16.9 (2.4)(4.1)(1.8)	**56.9** : 33.2 : 9.9 (1.8)(1.4)(0.4)	1 : 1	1 : 3
X	X	X	X	**54.3** : 14.3 : 13.0 : 18.4 (1.9)(0.2)(0.2)(1.8)	17.1 : **51.3** : 23.9 : 7.7 (1.8)(1.1)(0.7)(0.0)	2 : 3	1 : 3

4MP experiment produced crystals with the greatest amount of PYR, 96.2%. In the ternary experiments, 2MP remained favoured throughout, with selectivities ranging from 56.9% (2MP/3MP/4MP) to 67.9% (PYR/2MP/4MP). The absence of 2MP from the ternary solution then produced crystals with more of 3MP (PYR/3MP/4MP, 60.1%). Finally, the quaternary experiment predictably produced solids that contained a greater amount of 2MP (51.3%).

Overall, the affinity of **H2** was in the order 2MP > 3MP > PYR ≫ 4MP, where 4MP remained disfavoured throughout.

The overall H : G ratios for all of these complexes varied widely (Table 2).

Thus, the host compounds with oxygen or sulfur in the B rings of the tricyclic fused systems behaved very differently in these mixtures.

3.3 Binary non-equimolar mixed guest experiments

Host compounds **H1** and **H2** were subjected to crystallization experiments from non-equimolar binary guest solutions (80 : 20, 60 : 40, 40 : 60 and 20 : 80). The selectivity profiles (with the inserted 50 : 50 data points from the equimolar experiments, Table 2) are provided in Fig. 1 (**H1**) and 2 (**H2**). From a consideration of all of the data points in these plots were calculated the *K* values, which are summarized in Table 3 (where the percentage of the preferred guest in the original solution is provided in black bold text). The straight diagonal lines in these plots represent an unselective host compound (GC traces may be found in the SI).

In the PYR/2MP solutions (Fig. 1a), PYR was consistently favoured by **H1**, and the 80 : 20, 60 : 40 and 50 : 50 PYR/2MP experiments furnished significant *K* values, infinite, 24.0 and 13.3 (Table 3), alluding to feasible separations of these mixtures through supramolecular chemistry strategies (since *K* is required to be 10 or greater for efficient separations[46]). The host selectivity in the 40 : 60 and 20 : 80 PYR/2MP solutions was, however, more moderate ($K \leq 6.7$). The remaining five selectivity plots (Fig. 1b–f) indicate that the affinity behaviour of the host compound depended on the amounts of the two guest solvents present where, in each instance, the 20 : 80 experiment resulted in a selectivity towards the guest in the greater (80%) amount. More specifically, the 20 : 80 3MP/PYR experiment (Fig. 1b) saw more of PYR being enclathrated, and *K* was significant, 15.4, indicating that separations are plausible. However, the *K* values of the remaining data points, in favour of 3MP, were too low to suggest that successful separations are possible ($K \leq 4.9$). The most significant result in the PYR/4MP solutions (Fig. 1c) was the 60 : 40 experiment since *K* was calculated to be 13.2, while the 40 : 60, 50 : 50 and 80 : 20 PYR/4MP mixtures had *K* values that ranged between 2.9 and 8.7. Once more, in the 20 : 80 experiment, more of 4MP was selected, but *K* was only 1.5. The 3MP/2MP solutions (Fig. 1d) were in favour of 3MP when concentrations of this guest were 40% or more; *K* was, however, only 5.1 or less, while the 20 : 80 3MP/2MP experiment demonstrated a host affinity for 2MP ($K = 6.7$). Both Fig. 1e (4MP/2MP) and 1f (3MP/4MP), as was the case in Fig. 1d (3MP/2MP), afforded *K* values that were too low to allow for separations of these mixtures. From the

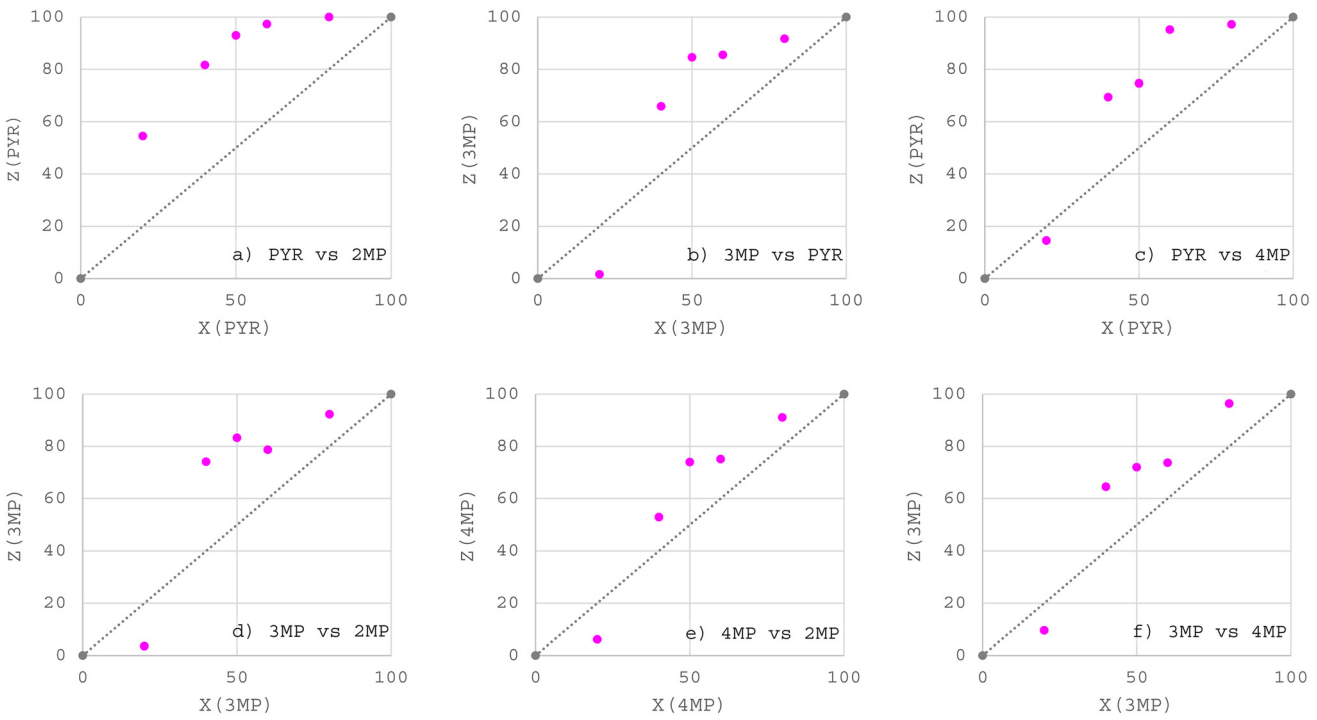

Fig. 1 Selectivity profiles obtained from the a) PYR/2MP, b) 3MP/PYR, c) PYR/4MP, d) 3MP/2MP, e) 4MP/2MP and f) 3MP/4MP binary solution experiments with **H1** as the host compound.

Table 3 Calculated *K* values in the binary guest experiments with **H1** and **H2**[a]

H1				**H2**			
PYR/2MP		3MP/2MP		2MP/PYR		2MP/3MP	
80:20	∞	**80**:20	3.0	**80**:20	3.5	**80**:20	6.9
60:40	**24.0**	**60**:40	5.1	**60**:40	2.7	**60**:40	3.9
50:50	**13.3**	**50**:50	5.0	**50**:50	2.8	**50**:50	2.3
40:60	6.7	**40**:60	4.3	**40**:60	2.3	40:**60**	2.2[a]
20:80	4.8	20:**80**	6.7[a]	20:**80**	**11.7**[a]	20:**80**	1.0[a]
3MP/PYR		4MP/2MP		3MP/PYR		2MP/4MP	
80:20	2.8	**80**:20	2.6	**80**:20	3.4	**80**:20	**22.5**
60:40	3.9	**60**:40	2.0	**60**:40	4.3	**60**:40	**9.6**
50:50	4.9	**50**:50	2.8	**50**:50	1.6	**50**:50	**11.3**
40:60	2.9	**40**:60	1.7	40:**60**	**41**[a]	**40**:60	**15.4**
20:**80**	**15.4**[a]	20:**80**	3.8[a]	20:**80**	∞[a]	**20**:80	**39.5**
PYR/4MP		3MP/4MP		PYR/4MP		3MP/4MP	
80:20	8.7	**80**:20	6.7	**80**:20	**10.6**	**80**:20	1.5
60:40	**13.2**[a]	**60**:40	1.8	**60**:40	**20.2**	**60**:40	2.4
50:50	2.9	**50**:50	2.6	**50**:50	**19.6**	**50**:50	3.0
40:60	3.4	**40**:60	2.7	**40**:60	**27.9**	**40**:60	4.2
20:**80**	1.5	20:**80**	2.4[a]	20:**80**	7.1[a]	**20**:80	**10.0**

[a] *K* values were calculated in favour of the preferred guest species in each experiment.

former plot (Fig. 1e, 4MP/2MP), for those experiments favouring 4MP, *K* values ranged between 1.7 and 2.8, while the 20:80 solution produced a solid with more of 2MP, but *K* was only 3.8. The latter plot (Fig. 1f, 3MP/4MP) produced *K* values between 1.8 and 6.7 when the selectivity was in favour of 3MP, while in the case in which more of 4MP was included (20:80 3MP/4MP), *K* was only 2.4.

Host compound **H2**, in low concentrations of 2MP in 2MP/PYR solutions (Fig. 2a, 20:80), demonstrated a preference for PYR, and the *K* value was notable, 11.7. The other data points in this plot, experiments which then favoured 2MP, however, provided *K* values that ranged between only 2.3 and 3.5, too low to allow for effective separations. Fig. 2b (3MP/PYR) also shows the selectivity behaviour of the host compound to be guest concentration dependent: from the 80:20, 60:40 and 50:50 3MP/PYR solutions were calculated *K* values between 1.6 and 4.3 (in favour of 3MP); however, as the concentration of PYR

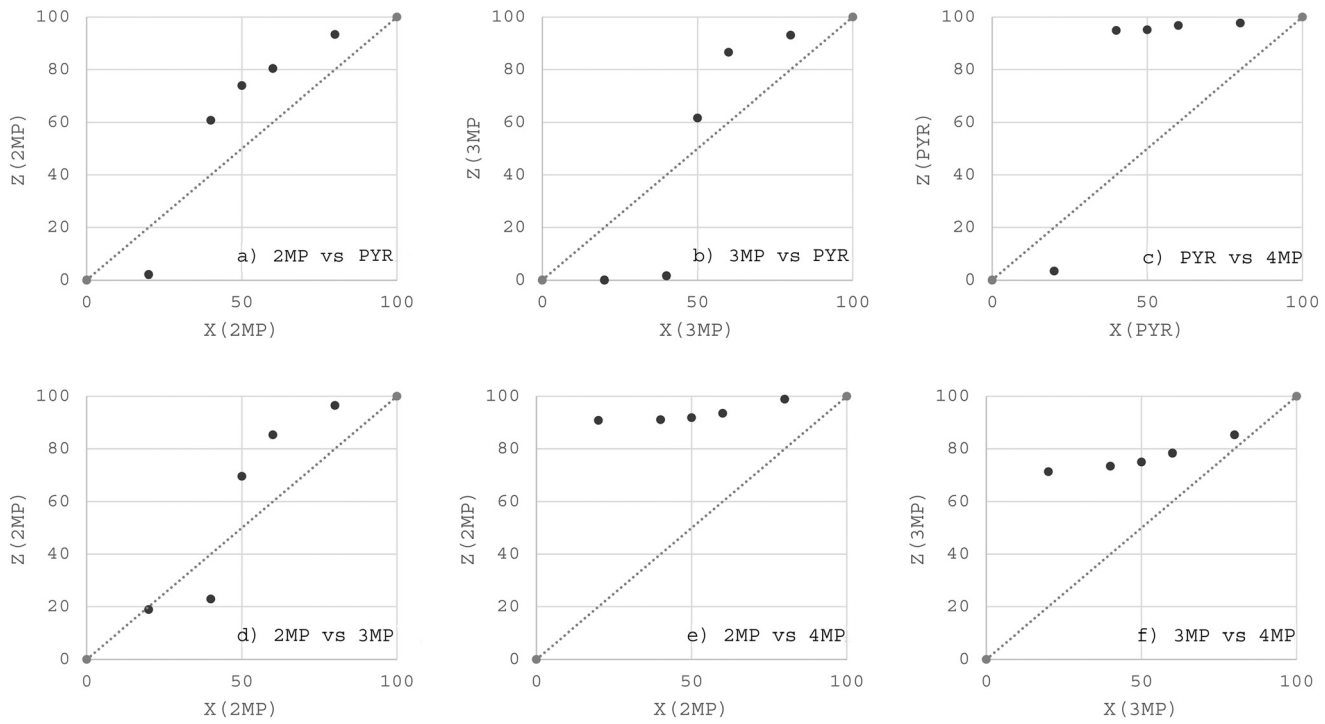

Fig. 2 Selectivity profiles obtained from the a) 2MP/PYR, b) 3MP/PYR, c) PYR/4MP, d) 2MP/3MP, e) 2MP/4MP and f) 3MP/4MP binary solution experiments with **H2** as the host compound.

increased (40 : 60 and 20 : 80 3MP/PYR), the selectivity (for PYR now) increased to overwhelming levels, and K was 41.0 and infinite in these two experiments, correspondingly. A consideration of the data provided in Fig. 2c (PYR/4MP) also demonstrated that at a low concentration of PYR (20 : 80 PYR/4MP), the host compound preferred 4MP (K = 7.1), while in the remaining solutions, K was prodigiously in favour of PYR, 10.6–27.9, and these solutions may be separated in this manner. The selectivity plot for the 2MP/3MP experiments (Fig. 2d) showed that the behaviour of **H2** was dependent upon the amounts of the two guests present once more. The 40 : 60 and 20 : 80 solutions produced crystals with more of 3MP, but K was low (2.2 and 1.0). In the other three experiments, 2MP was favoured, but K remained low (2.3–6.9). Fig. 2e (2MP/4MP) shows a consistent preference for 2MP in all instances; furthermore, all K values approached 10 or were significantly greater than 10 (9.6–39.5) and these solutions may be separated or purified in this particular fashion. Finally, the 3MP/4MP experiments (Fig. 2f) also demonstrated that 3MP was always favoured by **H2**, but only in the 20 : 80 3MP/4MP mixture was the K value high enough to allow for separations (K = 10.0). These values for the other data points were low, 1.5–4.2.

3.4 Thermal analyses

The T_{on} temperatures (the temperature at which guest desolvation commences and which serves as a measure of the relative thermal stability of the complex) were obtained through thermal analyses (Fig. 3a–h, where the TG curve is in

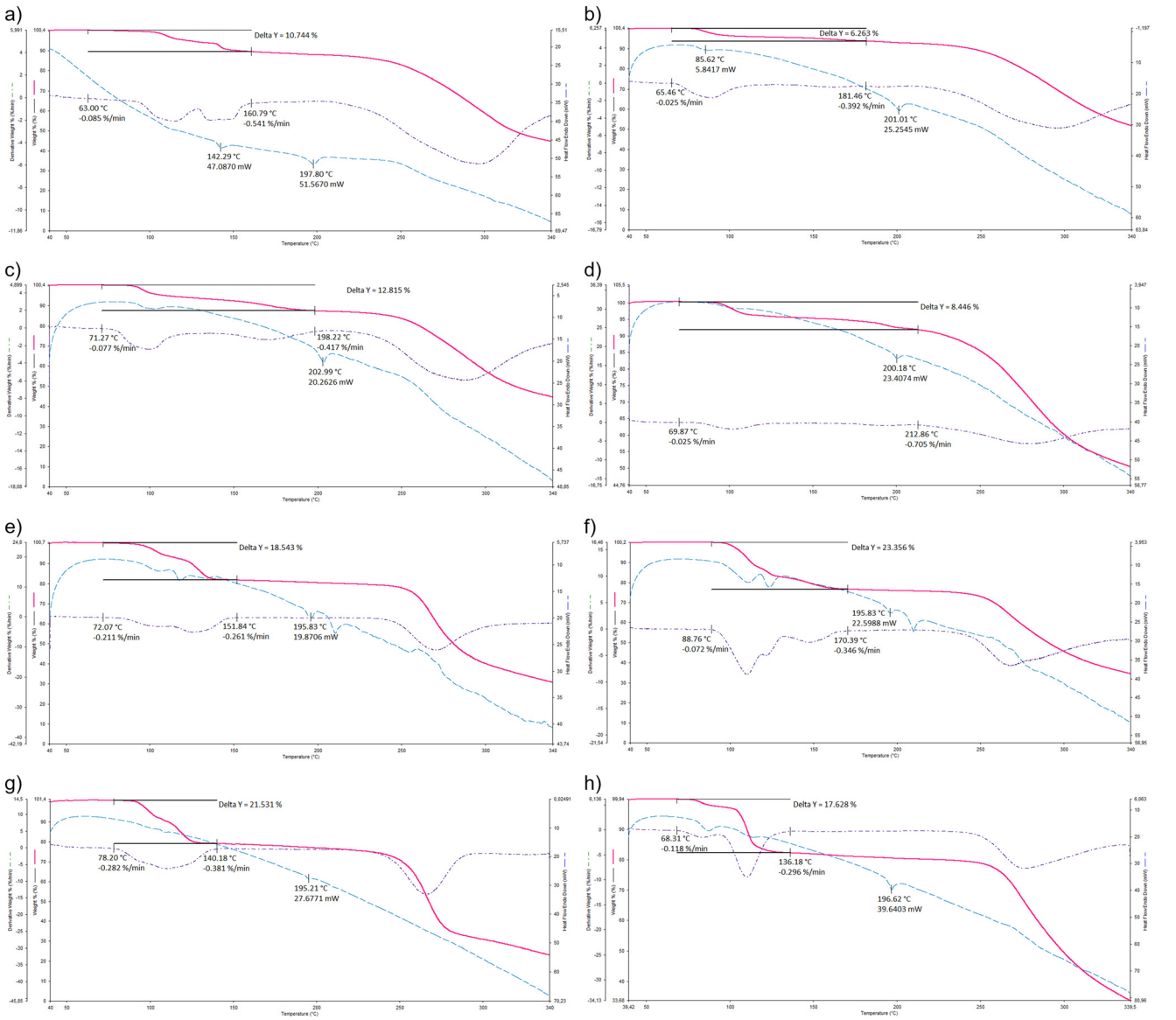

Fig. 3 Overlaid TG, dTG and DSC curves for a) **H1**·PYR, b) 2(**H1**)·2MP, c) **H1**·3MP, d) 2(**H1**)·4MP, e) **H2**·2(PYR), f) **H2**·2(2MP), g) **H2**·2(3MP) and h) 2(**H2**)·3(4MP).

Table 4 Thermal results for the pyridyl complexes of **H1** and **H2**[a]

Complex	T_{on}/°C	Experimental mass loss (%)	Predicted mass loss (%)
H1·PYR	63.0	10.7	10.5
2(**H1**)·2MP	65.5	6.3	6.5
H1·3MP	71.3	12.8	12.2
2(**H1**)·4MP	69.9	8.4	6.5
H2·2(PYR)	72.1	18.5	19.8
H2·2(2MP)	88.8	23.4	22.5
H2·2(3MP)	78.2	21.5	22.5
2(**H2**)·3(4MP)	68.3	17.6	17.9

[a] T_{on} is the onset temperature for the guest release process and serves as a measure of the thermal stability of the complex.

pink, the dTG in purple and the DSC in blue) and are provided in Table 4, together with the expected and measured mass losses, for the pyridyl complexes of **H1** and **H2**.

The predicted and expected mass losses for each of the eight complexes concurred reasonably well (Table 4), confirming the H : G ratios of the complexes as provided by the ^{1}H-NMR experiments (Table 1).

The preferred guest solvent of **H1** in the mixed guest competition experiments, 3MP, formed the most stable complex with this host compound, with a T_{on} temperature of 71.3 °C, while the remaining three complexes were less stable (T_{on} 63.0–69.9 °C). This observation explains the affinity of **H1** for 3MP. However, with PYR being preferred second to 3MP (3MP > PYR > 4MP ≫ 2MP), these thermal data do not provide an explanation for the entire selectivity order, since **H1**·PYR exhibited the lowest thermal stability of the four complexes (T_{on} 63.0 °C). As an explanation for this observation being perceived as a possible anomaly, it should be borne in mind that these thermal experiments were carried out on the single solvent complexes, whilst the host selectivity order was obtained from the guest competition experiments. Therefore, whilst it is often the case that the two sets of results concur with one another, it is not unexpected that this is not always the case, since the host compound is provided with very different conditions in the two experiments (in the guest competition and in the single solvent crystallization experiments).

Table 5 Relevant crystallographic parameters for the complexes of **H1** with the pyridines

	H1·PYR	2(**H1**)·2MP	**H1**·3MP	2(**H1**)·4MP
Chemical formula	$C_{40}H_{30}Cl_2N_2S_2{\cdot}C_5H_5N$	$2(C_{40}H_{30}Cl_2N_2S_2){\cdot}C_6H_7N$	$C_{40}H_{30}Cl_2N_2S_2{\cdot}C_6H_7N$	$2(C_{40}H_{30}Cl_2N_2S_2){\cdot}C_6H_7N$
Formula weight	752.78	1440.48	766.80	1440.48
Crystal system	Monoclinic	Triclinic	Monoclinic	Monoclinic
Space group	$P2_1/c$	$P\bar{1}$	$P2_1/c$	$P2_1/n$
μ (Mo-Kα)/mm^{-1}	0.331	0.339	0.328	0.339
a/Å	11.031(2)	11.2571(9)	12.1499(16)	27.4379(12)
b/Å	11.772(2)	23.2434(19)	10.8322(16)	11.5895(6)
c/Å	28.132(6)	29.357(3)	28.141(4)	44.419(2)
Alpha/°	90	113.227(4)	90	90
Beta/°	92.860(7)	94.356(4)	94.231(5)	95.0705(14)
Gamma/°	90	90.072(4)	90	90
V/Å^3	3648.4(13)	7034.3(11)	3693.6(9)	14 069.6(11)
Z	4	4	4	8
D(calc)/g cm^{-3}	1.370	1.360	1.379	1.360
F(000)	1568	3000	1600	6000
Temp./K	100	200	100	200
Restraints	0	28	6	679
N_{ref}	9098	28 832	9243	28 785
N_{par}	477	1819	489	1803
R	0.0328	0.0725	0.0354	0.0644
wR_2	0.0829	0.1697	0.0859	0.1714
S	1.03	1.05	1.02	1.07
θ min–max/°	1.9, 28.4	1.9, 26.5	2.0, 28.4	1.8, 26.4
Tot. data	139 350	394 762	159 150	435 231
Unique data	9098	28 832	9243	28 785
Observed data [$I > 2.0$ sigma(I)]	8276	24 209	7923	23 148
R_{int}	0.049	0.087	0.057	0.044
Completeness	0.995	0.999	0.999	0.999
Min. resd. dens. (e Å^{-3})	−0.34	−0.66	−0.48	−1.10
Max. resd. dens. (e Å^{-3})	0.40	0.53	0.50	0.72
CCDC number	2463136	2467552	2463135	2467553

Satisfyingly, a consideration of the T_{on} temperatures of the four pyridyl complexes of **H2** explains unambiguously the selectivity behaviour of this host compound in the crystallization experiments from mixed guests: this affinity order, 2MP > 3MP > PYR ≫ 4MP, is in direct accordance with the relative thermal stabilities of the complexes, with T_{on} being 88.8 °C (2MP) > T_{on} 78.2 °C (3MP) > T_{on} 72.1 °C (PYR) > T_{on} 68.3 °C (4MP). Therefore, 2MP was preferentially selected by **H2** since this guest solvent formed the complex with the greatest thermal stability of the four, while 4MP was not favoured since its complex with **H2** was the least stable one.

3.5 SCXRD analysis of the pyridyl inclusion compounds of H1 and H2

Tables 5 (**H1**) and 6 (**H2**) provide a summary of the relevant crystallographic parameters for the crystal structures of each of the eight complexes in the present investigation. Six of these, namely **H1**·PYR, **H1**·3MP, **H2**·2(PYR), **H2**·2(2MP), **H2**·2(3MP) and **H2**·2(4MP), crystallized in the monoclinic crystal system and space group $P2_1/c$, while the crystal structure of 2(**H1**)·4MP was also solved in the monoclinic crystal system but with the space group in the alternative setting of $P2_1/c$, namely $P2_1/n$. 2(**H1**)·2MP, on the other hand, crystallized in the triclinic crystal system and space group $P\bar{1}$. Note that the crystal selected for SCXRD analysis of the inclusion compound of **H2** with 4MP had a 1 : 2 H : G ratio, which differed slightly (2 : 3) from that which was observed in both ^{1}H-NMR and TG analyses.

The unit cell of the complex **H1**·PYR was composed of one non-centrosymmetric host molecule and a single guest species. The diamino linker of the host compound assumed a folded configuration with a N–C–C–N torsion angle of −72.0(1)°, that is, the NH moieties were oriented almost gauche with respect to one another when the carbons between them were overlaid; moreover, no structural disorder was evident. The unit cells of 2(**H1**)·2MP and 2(**H1**)·4MP, on the other hand, each had four host molecules. In the former instance, two host species had folded linkers (the torsion angles between the NH groups were nearly gauche and measured 70.5(6) and 70.8(6)°), while the remaining two host molecules had their linkers in an extended conformation (torsion angles approached an anti-periplanar configuration, 176.3(4) and 178.5(5)°). In 2(**H1**)·4MP, the linkers of three of the host molecules were folded (−72.2(3), −73.7(3) and 74.6(3)°), while one host molecule presented an extended linker (171.4(3)°). In the complex **H1**·3MP, the asymmetric unit consisted of one host molecule and one guest molecule, and the linker was in an extended conformation (179.6(1)°). The guest molecule was ordered, but a pair of disordered

Table 6 Relevant crystallographic parameters for the complexes of H2 with the pyridines

	H2·2(PYR)	**H2**·2(2MP)	**H2**·2(3MP)	**H2**·2(4MP)
Chemical formula	$C_{40}H_{30}Cl_2N_2O_2{\cdot}2(C_5H_5N)$	$C_{40}H_{30}Cl_2N_2O_2{\cdot}2(C_6H_7N)$	$C_{40}H_{30}Cl_2N_2O_2{\cdot}2(C_6H_7N)$	$C_{40}H_{30}Cl_2N_2O_2{\cdot}2(C_6H_7N)$
Formula weight	799.76	827.81	827.81	827.81
Crystal system	Monoclinic	Monoclinic	Monoclinic	Monoclinic
Space group	$P2_1/c$	$P2_1/c$	$P2_1/c$	$P2_1/c$
μ (Mo-Kα)/mm^{-1}	0.208	0.208	0.209	0.206
a/Å	10.2394(4)	10.1122(4)	10.2840(4)	14.8825(6)
b/Å	25.2702(10)	25.887(1)	25.5527(9)	11.6416(4)
c/Å	7.8761(3)	7.8505(3)	7.8072(3)	24.0763(8)
Alpha/°	90	90	90	90
Beta/°	97.0302(14)	96.923(2)	97.384(1)	98.279(1)
Gamma/°	90	90	90	90
V/Å^3	2022.63(14)	2040.09(14)	2034.59(13)	4127.9(3)
Z	2	2	2	4
D(calc)/g cm^{-3}	1.313	1.348	1.351	1.332
F(000)	836	868	868	1736
Temp./K	200	100	100	100
Restraints	72	0	0	0
N_{ref}	5022	5072	4508	10 302
N_{par}	310	276	276	551
R	0.0527	0.0375	0.0372	0.0373
wR_2	0.0999	0.0850	0.0764	0.0926
S	1.15	1.04	1.04	1.04
θ min–max/°	2.2, 28.3	2.0, 28.3	2.0, 27.2	1.9, 28.4
Tot. data	59 158	57 795	55 689	195 964
Unique data	5022	5072	4508	10 302
Observed data [I > 2.0 sigma(I)]	3649	4247	3576	8413
R_{int}	0.083	0.060	0.079	0.071
Completeness	0.998	0.998	0.999	0.998
Min. resd. dens. (e Å^{-3})	−0.28	−0.28	−0.24	−0.28
Max. resd. dens. (e Å^{-3})	0.27	0.29	0.24	0.37
CCDC number	2463337	2463137	2463139	2463141

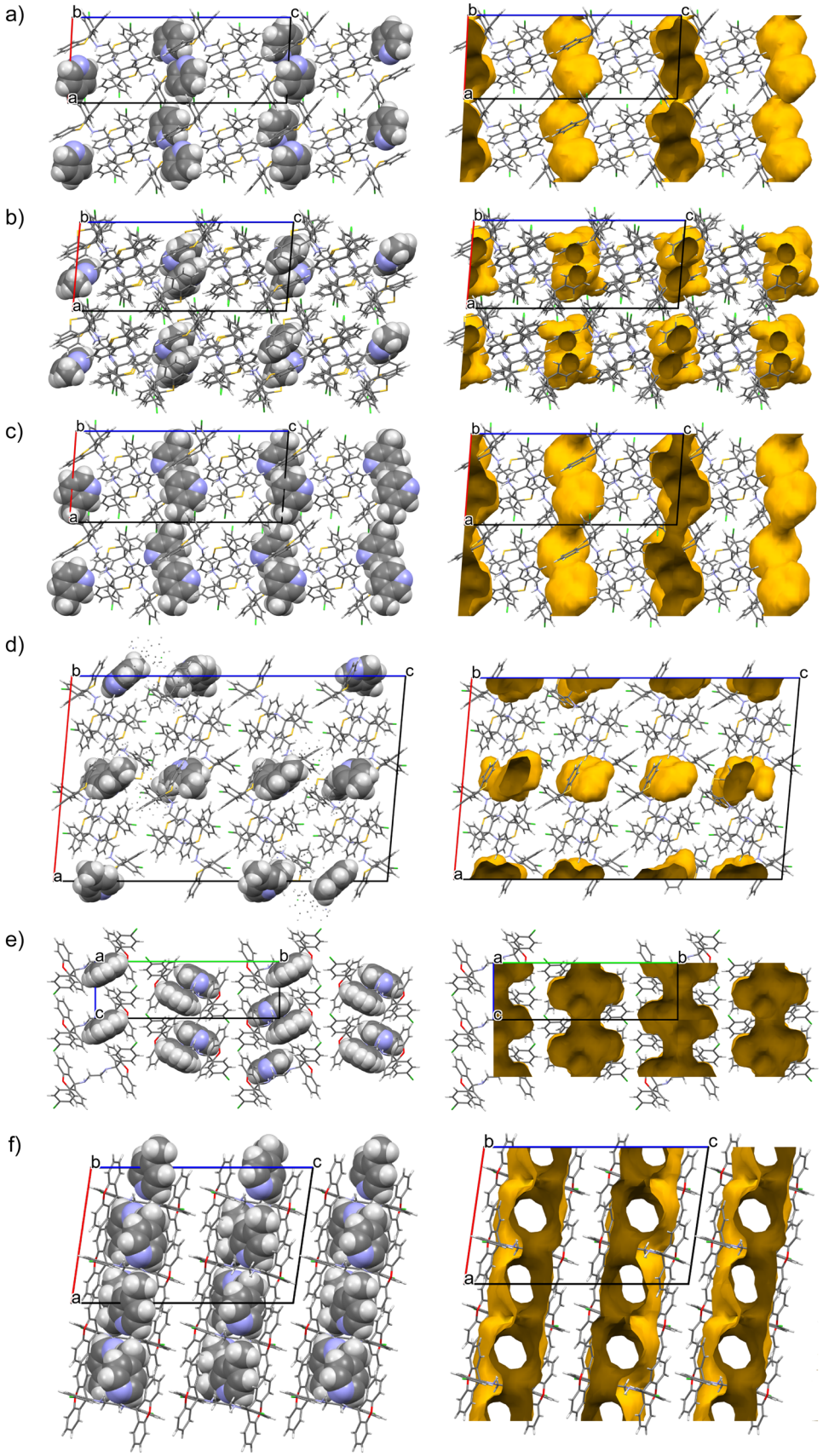

Fig. 4 Unit cell and host–guest packing (left) and void (right) diagrams for a) **H1**·PYR [010], b) 2(**H1**)·2MP [010], c) **H1**·3MP [010], d) 2(**H1**)·4MP [010], e) **H2**·2(PYR) [100] (which represents also **H2**·2(2MP) and **H2**·2(3MP), as they are isostructural) and f) **H2**·2(4MP) [010]. Guest molecules are in space-filling and host species are in stick representations.

hydrogen atoms was located on one of the nitrogen atoms of the host molecule (when considering the difference Fourier map); the major hydrogen atom component had a refined occupancy of 0.53.

In the unit cell of **H2**·2(PYR), some disorder in the guest molecule was evident, while in **H2**·2(2MP), the host molecule was located on a centre of inversion and the guest species was situated in a general position, which was then repeated by the inversion centre, resulting in the 1 : 2 H : G stoichiometry. The asymmetric unit of clathrate **H2**·2(3MP) consisted of one half of a host molecule and one guest molecule; the host species was, once more, positioned on a centre of inversion and the guest in a general position. The chemical formula unit was thus one centrosymmetric host molecule and two inversion-related guest molecules. Finally, the unit cell in **H2**·2(4MP) had a host molecule with pseudo-centrosymmetry and two guest molecules that adopted pseudo-centrosymmetric positions around the host species.

The nature of the guest accommodation in the eight complexes was subsequently scrutinized after deleting the guest molecules from the packing calculations. In **H1**·PYR and **H1**·3MP, the guest molecules occupied constricted channels (Fig. 4a and c, respectively). In fact, in the former complex, these channels were extremely constricted and may even be regarded as discrete cavities with two guest molecules residing in each one. Initially, when noting their similar unit cell dimensions, it was thought that these two complexes shared a common host packing. However, by comparing their calculated PXRD patterns (Fig. 5a), this was clearly not the case which, in hindsight, was not surprising given the very different geometries of the linkers of the host molecules (folded *vs.* extended). The guest species in both 2(**H1**)·2MP and 2(**H1**)·4MP were located in discrete cavities (Fig. 4b and d). The host packing in complexes **H2**·2(PYR), **H2**·2(2MP) and **H2**·2(3MP) was, however, isostructural, as confirmed by their comparable unit cell dimensions (Table 6) and their stacked PXRD patterns (calculated after guest deletion) as provided in Fig. 5b. Their guests occupied infinite unidirectional channels, with Fig. 4e, for **H2**·2(PYR), being representative of the other two complexes as well.

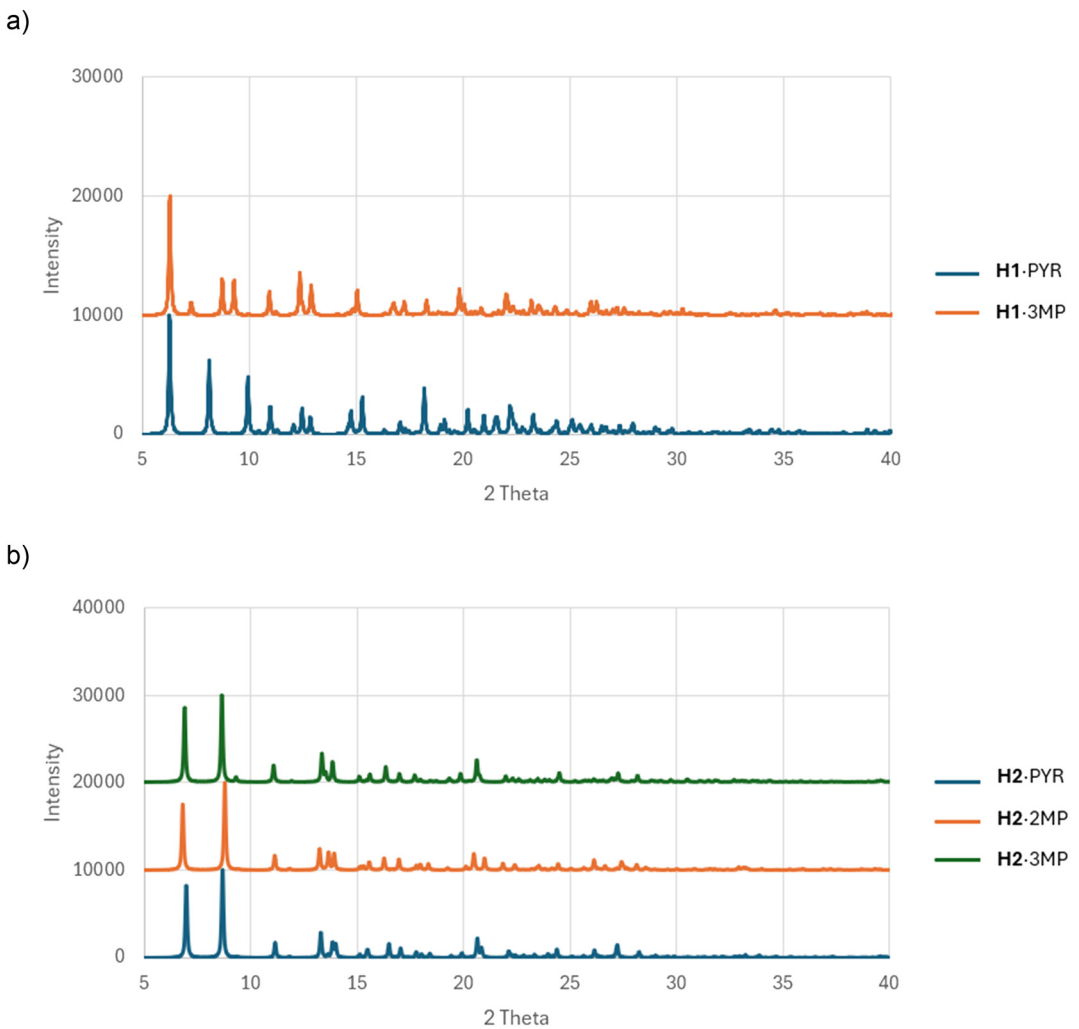

Fig. 5 Calculated PXRD patterns demonstrating that a) **H1**·PYR and **H1**·MP do not share a common host packing, while b) **H2**·2(PYR), **H2**·2(2MP) and **H2**·2(3MP) do.

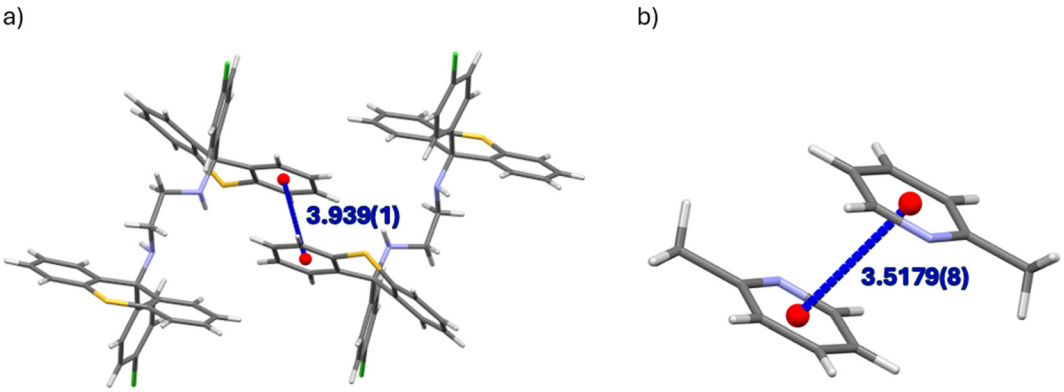

Fig. 6 The intermolecular π···π stacking interaction between a) two **H1** host molecules in **H1**·PYR and b) two 2MP guest molecules in **H2**·2(2MP). Guest and host molecules, respectively, have been deleted for clarity.

Finally, in **H2**·2(4MP), the guests were located in multidirectional channels (Fig. 4f). These latter observations explain the affinity behaviour of **H2** for 2MP, while continually disfavouring 4MP: complexes with guests in multidirectional channels usually exhibit lower thermal stabilities compared with when the guests are in unidirectional channels, as was confirmed earlier by the thermal analysis results for these complexes of **H2**.

Of the four complexes of **H1**, only **H1**·PYR and 2(**H1**)·4MP experienced π···π interactions and these were observed between host molecules only. In the former case, one such interaction was identified, with a centroid···centroid (Cg···Cg) distance of 3.939(1) Å and a slippage of 1.926 Å (Fig. 6a). However, in the latter inclusion compound, four interactions of this type were observed, and their Cg···Cg distances ranged between 3.528(6) and 3.726(8) Å. In **H2**·2(PYR) and **H2**·2(2MP), furthermore, were also observed π···π short contacts, but these were between guest molecules only; their Cg···Cg distances were between 3.5179(8) and 3.829(8) Å (with slippages between 0.917 and 1.676 Å). An example is provided in Fig. 6b.

Table S1 (in the SI) summarizes the parameters for the multitude of C–H···π interactions identified in each of the four complexes of **H1** and **H2**, with many more of these short contacts in the complexes of the former host compound compared with those in the latter. These were observed within host molecules, between them, between guest molecules and between host and guest species, and stabilized the packing of the molecules in the crystals of their complexes and, also, facilitated guest retention. In those complexes involving **H1**, the distances of these close contacts ranged between 2.59 and 2.99 (H···π), and 3.386(4) and 3.850(8) (C···π) Å, with angles between 111 and 172°. These interactions in the complexes with **H2** were between 2.78 and 2.98 (H···π), and 3.456(2) and 3.856(2) (C···π) Å; applicable angles ranged between 115 and 173°. Interestingly, the preferred guest of **H1**, 3MP, experienced three of these interactions with the host molecule, while consistently disfavoured 2MP did not interact in this way with **H1**. **H2**, on the other hand, always interacted in this manner with each of the four guest solvents. Examples of these are provided in Fig. 7: Fig. 7a shows the intramolecular interaction of this

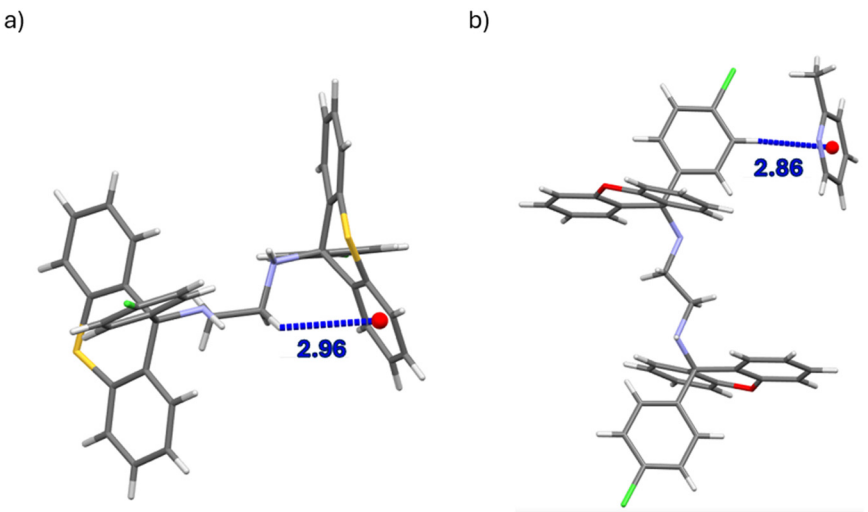

Fig. 7 The C–H···π interactions present in a) **H1**·PYR and in b) **H2**·2(2MP), as examples.

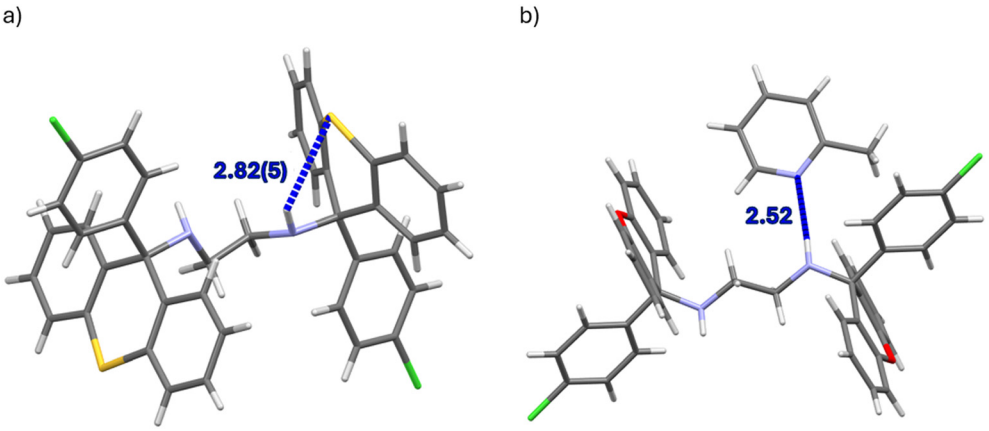

Fig. 8 The classical a) N–H···S and b) N–H···N hydrogen bonding interactions present in complexes 2(**H1**)·2MP and **H2**·2(2MP), respectively.

type between the hydrogen atom of the CH_2 moiety of the diamino linker (in **H1**·PYR) and one of the aromatic rings of the tricyclic fused system and Fig. 7b demonstrates this close contact between the free host aromatic group and the centroid of the guest species in **H2**·2(2MP).

The applicable parameters of the inter- and intramolecular hydrogen bonding interactions identified in the eight complexes of the present investigation, both classical and non-classical, are summarised in Table S2 (SI), where D is the donor atom and A is the acceptor atom. Classical intermolecular (host)N–H···N(guest) hydrogen bonding close contacts, facilitating guest retention, were identified in each of the **H2**·2(PYR), **H2**·2(2MP) and **H2**·2(3MP), with two of these in **H2**·2(PYR). These measured between 2.355(18) and 2.520(17) Å (H···N), with N···N distances ranging between 3.25(1) and 3.401(2) Å; the bond angles were 172(1)–176(2)°.

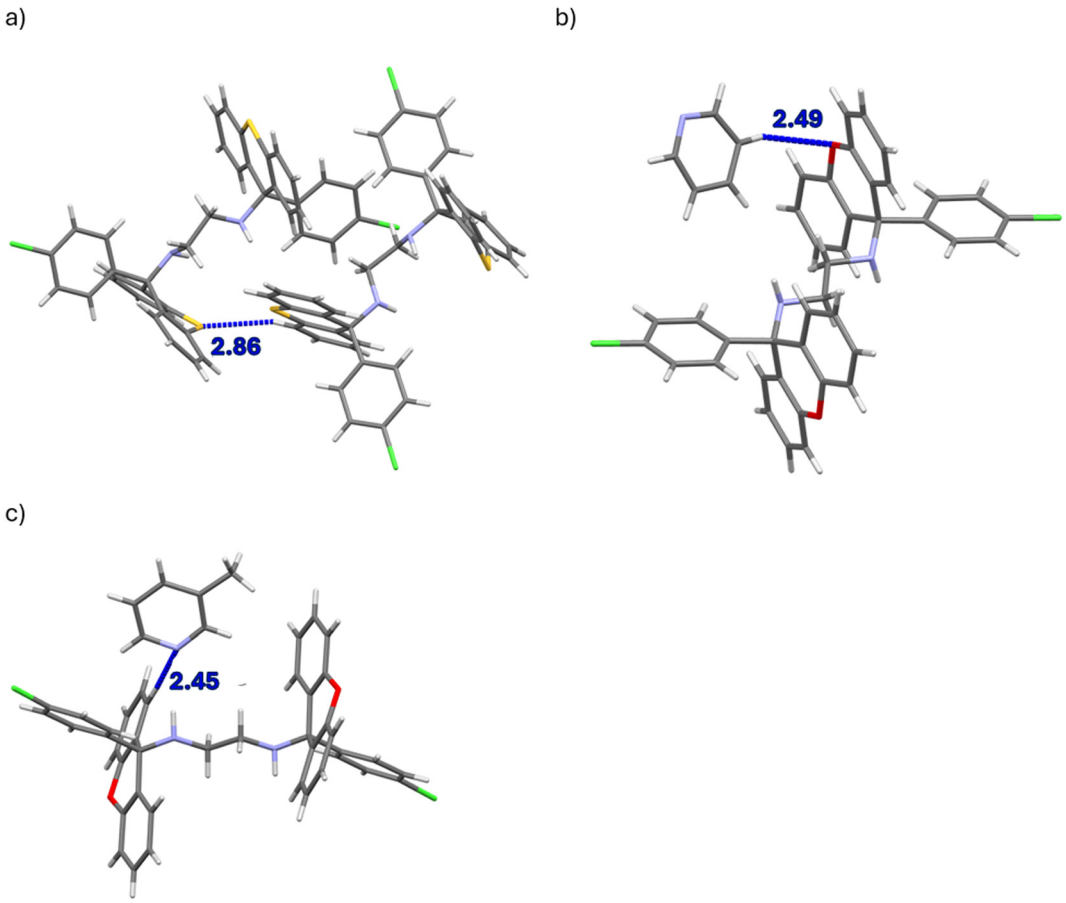

Fig. 9 Non-classical intermolecular hydrogen bonding in complexes a) **H1**·PYR, b) **H2**·2(PYR) and c) **H2**·2(3MP).

Interestingly, these types of short contacts were not observed in any of the complexes with **H1** nor in **H2**·2(4MP). However, in the 2(**H1**)·2MP inclusion compound, and only in this one, were noted (host)N–H···S(host) interactions, which were classical and intramolecular in nature, and assisted in stabilizing the geometry of the host molecule, thus reducing its flexibility; applicable parameters for H···N were 2.82(5) and 2.86(5) Å, and for N···S 3.422(5) and 3.447(5) Å, and the bond angles were 127(4) and 125(4)°, correspondingly. Non-classical intermolecular (guest)C–H···S(host) and (host)C–H···S(host), as well as three non-classical intramolecular (host)C–H···S(host), interactions were also identified. The intermolecular (guest)H···S(host) and (host)H···S(host) bond lengths were 2.86 Å and between 2.80 and 2.86 Å, (guest) C···S(host) and (host)C···S(host) 3.712(8) Å and between 3.723(4) and 3.773(3) Å, and the bond angles were 145° and between 159 and 165°, respectively. Those intramolecular in nature within host molecules measured 2.80–2.81 Å (H···S) and 3.548(2)–3.581(7) Å (C···S); 136–140° were the bond angles. A number of non-classical hydrogen bonds were also observed in these complexes, of the C–H···N type, both inter- and intramolecular, and were responsible for guest retention in the crystals, stabilization of the host packing motif and the host molecular geometry. These intramolecular host close contacts measured between 2.37 and 2.50 (H···N), and 2.748(9) and 2.846(3) (C···N) Å (100–104°). Those between host molecules and between host and guest species measured between 2.43 and 2.71 Å (H···N), and 3.285(5) and 3.514(9) (C···N) Å. The bond angles were 126–176°. Finally, two non-classical intermolecular (guest)C–H···O(host) and (host)C–H···O(host) interactions were identified in complexes **H2**·2(PYR), **H2**·2(3MP) and **H2**·2(4MP), where the H···O distances were 2.49 Å and between 2.51 and 2.69 Å, correspondingly; C···O measured 3.37(1) Å and between 3.253(2) and 3.318(2) Å, and bond angles were 154° and between 127 and 137°. In Fig. 8a is illustrated the host diamino linker NH group interacting with the sulfur atom of the tricyclic fused system, while Fig. 8b depicts the NH group in close contact with the nitrogen of the guest species. Non-classical intermolecular interactions, specifically C–H···S (**H1**·PYR), C–H···O (**H2**·2(PYR)) and C–H···N (**H2**·2(3MP)), are illustrated in Fig. 9. In Fig. 9a, a hydrogen of the aromatic ring of the tricyclic fused system interacts with another sulfur atom of the tricyclic fused system of another host molecule. Fig. 9b is a depiction of a hydrogen atom of the guest molecule interacting with the oxygen atom of the tricyclic fused system, and Fig. 9c shows a hydrogen on the aromatic ring of the tricyclic fused system interacting with the nitrogen of a guest molecule. The intramolecular (host)C–H···N(host) (left) and (host)C–H···S(host) (right) close contacts are provided in Fig. 10, where in both cases the hydrogen atom of the free aromatic ring interacts with the nitrogen atom of the diamino linker (Fig. 10a) and the sulfur atom of the tricyclic fused system (Fig. 10b).

Other short contacts, which occurred in all four **H1** complexes and the **H2**·2(4MP) inclusion compound, with distances less than the sum of the van der Waals radii (<) of the involved atoms or this sum minus 0.2 Å (≪), are provided in Table S3 of the SI. These interactions were largely of the (host)C–H···C–C(host), (guest)C–H···C–C(host), (host)C–H···C–Cl(host), (guest)C–H···C–Cl(host), (host)C–H···C–S(host) and (host)C–H···C–C(guest) types. The H···C distances measured between 2.49 and 2.94 Å (114–169°). An example of the (host)C–H···C–C(host) interaction is provided in Fig. 11a (**H1**·PYR), (host)C–H···C–Cl(host) in Fig. 11b (2(**H1**)·2MP), and (guest)C–H···C–Cl(host) in Fig. 11c (**H1**·3MP). The distances of the applicable interactions were 2.89, 2.80 and 2.80 Å, with bond angles of 134, 131 and 140°.

In summary, it was challenging singling out the short contacts responsible for the affinity behaviour of **H1** and **H2** in guest mixtures owing to the extremely large number and variety of noncovalent interactions present in these complexes (Tables S1–S3 in the SI). Only the PYR-, 2MP- and 3MP-containing complexes of the latter host species experienced classical hydrogen bonds between the host and guest molecules, which were absent in all of the complexes with **H1** and also in **H2**·2(4MP). However, the disfavoured guest of **H1**, 2MP, did not interact with the host species through C–H···π contacts, while its preferred guest solvent,

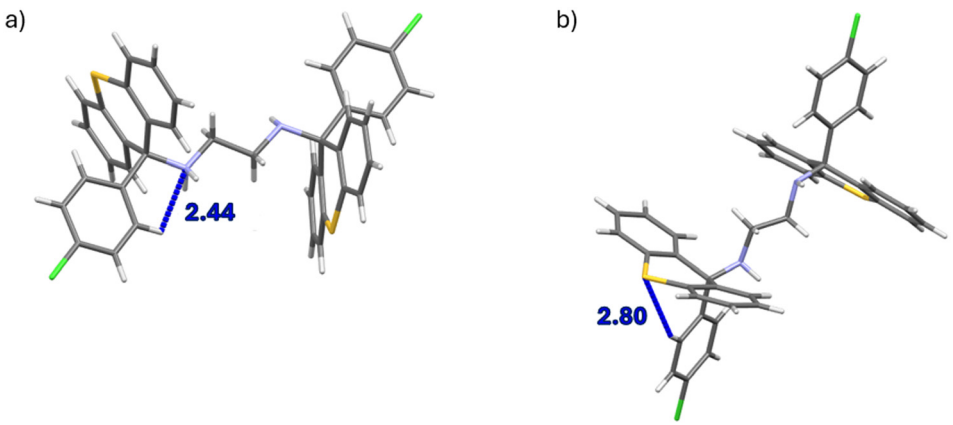

Fig. 10 Non-classical intramolecular hydrogen bonding, a) (host)C–H···N(host) and b) (host)C–H···S(host).

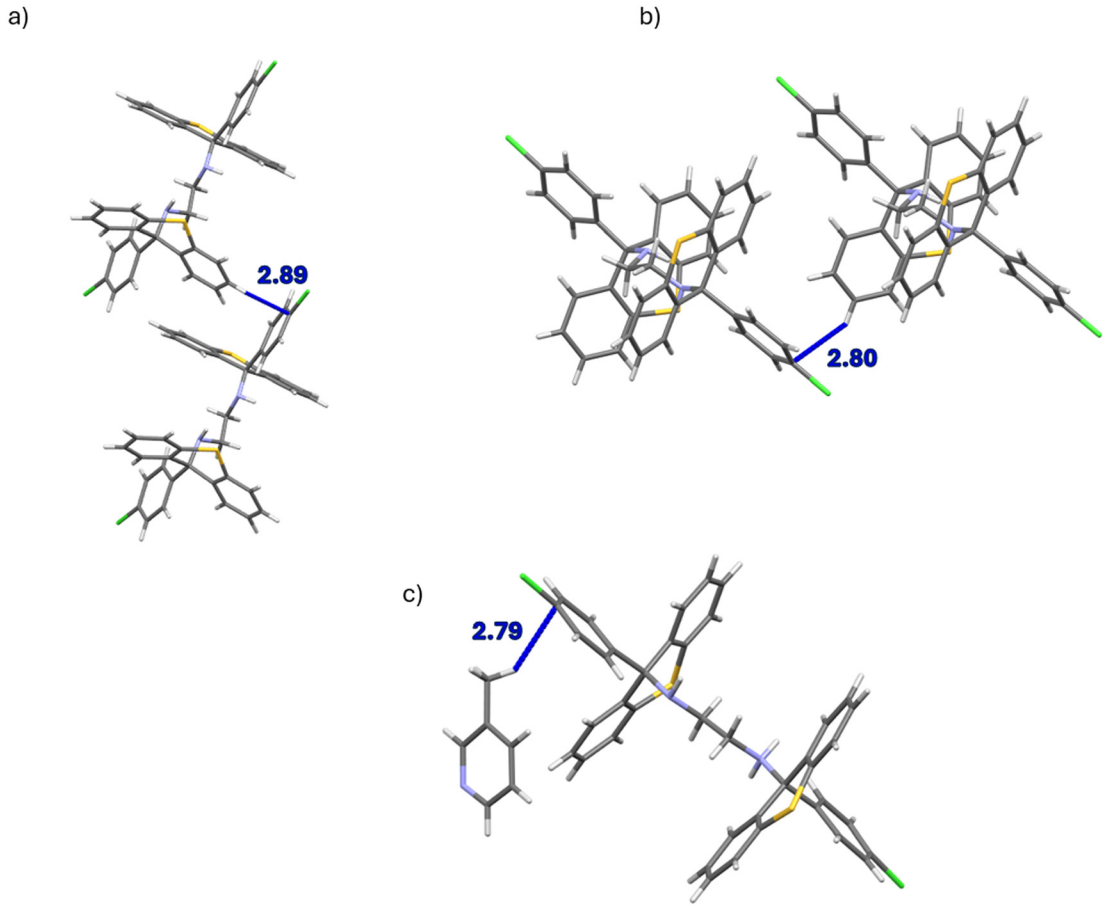

Fig. 11 Other short contacts in a) 2(**H1**)·2MP, b) **H1**·PYR and c) **H1**·3MP.

3MP, experienced three such close contacts, one (host)C–H···π(guest) (2.76, 3.582(2) Å and 145°) and two (guest)C–H···π(host) (2.75 and 2.83 Å, 3.711(2) and 3.738(2) Å, and 168 and 154°) in nature. This observation plausibly explains the affinity of **H1** for 3MP and its consistently low selectivity for 2MP. Furthermore, **H2** accommodated preferred 2MP in unidirectional channels, while 4MP, which was always disfavoured, was housed in multidirectional channels. This may explain the selectivity behaviour of this host species: multidirectional channel occupation is associated with lower complex stabilities when compared with unidirectional channel housing, and this is supported by the results from thermal analysis, where the 4MP-containing complex was observed to be the least stable of the four inclusion compounds.

4. Conclusions

Host compounds **H1** and **H2** were demonstrated to possess the ability to form complexes with each of the PYR and MPs, with H : G ratios varied. The equimolar guest competition experiments demonstrated that the selectivities of these host compounds for these guest solvents were in the order 3MP > PYR > 4MP ≫ 2MP and 2MP > 3MP > PYR ≫ 4MP, respectively. The binary guest competition experiments revealed that, in the case of **H1**, the 80 : 20, 60 : 40 and 50 : 50 PYR/2MP (K = ∞/24.0/13.3, in favour of PYR), 20 : 80 3MP/PYR (K = 15.4, favouring PYR) and 60 : 40 PYR/4MP (K = 13.2 for PYR) may all be effectively separated by means of supramolecular chemistry strategies. **H2** behaved even more selectively, and each of the 20 : 80 2MP/PYR (K = 11.7, preferring PYR), 40 : 60 and 20 : 80 3MP/PYR (K = 41/∞, PYR), all mixtures of PYR/4MP but the 20 : 80 combination (K = 10.6/20.2/19.6/27.9, in favour of PYR), all combinations of 2MP/4MP (K = 22.5/9.6/11.3/15.4/39.5, for 2MP) and, finally, 20 : 80 3MP/4MP (K = 10.0, preferring 3MP) mixtures may be purified in this fashion. Thermal analyses showed that the complex with the favoured guest of **H1**, 3MP, was the most stable one with the highest T_{on} (71.3 °C), explaining the affinity of this host species for 3MP. These analyses also clarified why 2MP was preferred by **H2**; this complex also had the highest T_{on} (88.8 °C), while the least favoured guest solvent, 4MP, formed an inclusion compound with the lowest T_{on} (68.3 °C). In all eight complexes, through SCXRD analyses, were observed a myriad of short noncovalent interactions which served to stabilise these inclusion compounds. This analytical technique provided reasons for the host affinity behaviour when crystallized from guest mixtures. In the complex of **H1** with preferred 3MP were identified three C–H···π close contacts between host and

guest species, while disfavoured 2MP did not interact with the host molecule in this manner. Furthermore, **H2** exhibited an enhanced selectivity for 2MP as a result of the higher thermal stability of this complex due to its guest accommodation in unidirectional channels, compared with 4MP, never being preferentially selected by **H2**, which was housed in wide open multidirectional channels and, as a consequence, exhibited the lowest thermal stability of the four.

Author contributions

D. B. T.: investigation; methodology; validation; data collection. B. B.: conceptualization; funding acquisition; methodology; project administration; resources; supervision; visualization; writing – original draft. M. R. C.: resources; assistance with the original draft; data curation; formal analysis. E. C. H.: data curation; formal analysis.

Conflicts of interest

There are no conflicts of interest to declare.

Data availability

The crystal structures of complexes **H1**·PYR, 2(**H1**)·2MP, **H1**·3MP, 2(**H1**)·4MP, **H2**·2(PYR), **H2**·2(2MP), **H2**·2(3MP) and **H2**·2(4MP) were deposited at the Cambridge Crystallographic Data Centre (CCDC) and their CCDC numbers are 2463136, 2467552, 2463135, 2467553, 2463337, 2463137, 2463139 and 2463141, respectively.

Supplementary information: the supporting information (SI) section contains the applicable ^{1}H-NMR spectra, GC traces and comprehensive data tables populated with the noncovalent interactions in these eight complexes. See DOI: https://doi.org/10.1039/d5ce00969c.

CCDC 2463135–2463137, 2463139, 2463141, 2463337, 2467552 and 2467553 contain the supplementary crystallographic data for this paper.[48a–h]

Acknowledgements

Financial support from the Nelson Mandela University is acknowledged, and B. B. also thanks the National Research Foundation (South Africa) as does D. B. T. (NRF grant number PMDS22052414135). M. R. C. thanks the University of Cape Town for access to research facilities at the Department of Chemistry.

References

1 R. N. Bhattacharya, M. B. Roy, S. N. Banerjee and G. C. Nandi, Recovery, purification and utilization of pyridine bases from coke oven by-products, *Ultimate Res. J. Ayurved*, 1982, **11**, 215–240.
2 A. E. Tschitschibabin, Über kondensation der aldehyde mit ammoniak zu pyridinbasen, *J. Prakt. Chem.*, 1924, **107**, 122–128.
3 J. J. Li, Chichibabin pyridine synthesis, in *Name Reactions*, Springer, Berlin, Heidelberg, 2009, pp. 107–109.
4 R. L. Frank and R. P. Seven, Pyridines. IV. A study of the Chichibabin synthesis, *J. Am. Chem. Soc.*, 1949, **1949**(71), 2629–2635.
5 S. Shimizu, N. Watanabe, T. Kataoka, T. Shoji, N. Abe, S. Morishita and H. Ichimura, Pyridine and pyridine derivatives, in *Ullmann's Encyclopedia of Industrial Chemistry*, Wiley-VCH, Weinheim, 2000.
6 *Pyridine [Internet]*, ed. P. P. Pandey, InTech, 2018, Available from: DOI: 10.5772/intechopen.71351.
7 N. C. Desai, J. D. Monapara, A. M. Jethawa and U. Pandit, Contemporary development in the synthesis and biological applications of pyridine-based heterocyclic motifs, in *Recent Developments in the Synthesis and Applications of Pyridines*, Elsevier, 2023, pp. 253–298.
8 S. De, S. K. A. Kumar, S. Kumar Shah, S. Kazi, N. Sarkar, S. Banerjee and S. Dey, Pyridine: The scaffolds with significant clinical diversity, *RSC Adv.*, 2022, **12**, 15385–15406.
9 Z. Yin, Y. Cao, W. Sun, G. Chen, X. Fang and L. He, 3-Methylpyridine: Synthesis and applications, *Chem. – Asian J.*, 2024, **19**, e202400467.
10 N. Toru, M. Caluwadewa Deepal, M. Jacques and Y. Hideaki, Nitrile hydratase-catalyzed production of nicotinamide from 3-cyanopyridine in rhodococcus rhodochrous J1, *Appl. Environ. Microbiol.*, 1988, **54**, 1766–1769.
11 L. Hilterhaus and A. Liese, Building blocks, in *White Biotechnology. Advances in Biochemical Engineering/Biotechnology*, ed. R. Ulber and D. Sell, Springer Science & Business Media, 2006, vol. 105, pp. 133–173.
12 J. W. Schmidberger, L. J. Hepworth, A. P. Green and S. L. Flitsch, Enzymatic Synthesis of Amides, in *Biocatalysis in Organic Synthesis 1. Science of Synthesis*, ed. K. Faber, W.-D. Fessner and N. J. Turner, Georg Thieme Verlag, 2015, pp. 329–372.
13 *CRC Handbook of Chemistry and Physics*, ed. W. M. Haynes, CRC Press, 97th edn, 2016.
14 H. A. Kooijman and E. Sorensen, Recent advances and future perspectives on more sustainable and energy efficient distillation processes, *Chem. Eng. Res. Des.*, 2022, **188**, 473–482.
15 C. Chang, T. Qiu, C. Yang, Z. Lei, W. Mo, H. Tao, B. Wang, X. Hu and W. Shen, A general distillation strategy and energy-efficient process design for optimal sequence screening in complicated homologue-azeotrope coexisting system, *Sep. Purif. Technol.*, 2025, **364**, 132204.
16 Y. Zeng, C. Liang, X. Lu, L. Zhao, F. Wu, T. Hou, A. Zhao, M. Lv, Z. Tao and Q. Li, Perfect separation of pyridine and 3-methylpyridine by cucurbit[6]uril, *Chin. Chem. Lett.*, 2025, **36**, 110807.
17 S. Neshati and Z. Hashisho, Adsorption dynamics of aromatic and polar volatile organic compounds on metal-organic frameworks, *Microporous Mesoporous Mater.*, 2025, **391**, 113619.
18 I. Miyoshi, H. Sonehara, J. Ogihara, T. Matsumoto, N. Morohashi and T. Hattori, Inclusion of amine isomers with

open-chain hosts having a partial structure of p-tert-butylthiacalixarene, *J. Org. Chem.*, 2021, **86**, 7046–7058.
19 P. Bednář, Z. Stránský, P. Barták and P. Adamovský, Polyethylene glycol as a separation medium for capillary zone electrophoretic analysis of pyridine derivatives, *J. Chromatogr. A*, 1999, **838**, 89–99.
20 Y. S. Sotnikova, Y. V. Patrushev, V. N. Sidelnikov and A. A. Mazaeva, In situ functionalization of HPLC monolithic columns based on divinylbenzene-styrene-4-vinylbenzyl chloride, *Talanta*, 2020, **220**, 121400.
21 A. H. Abdelhay and A. D. Bani-Yaseen, Recent advances and perspectives of supramolecular host-guest systems for electrochemical energy storage, *Mater. Today Chem.*, 2024, **40**, 102259.
22 A. Pakhomova, B. Journaux, A. Kurnosov, T. B. Ballaran, G. Tobie and M. Hanfland, Methanol storage in high-pressure clathrate hydrates as a prolonged source of methane in large ocean worlds, *Earth Planet. Sci. Lett.*, 2025, **666**, 119478.
23 E. J. Beckwée, G. V. Baron and J. F. M. Denayer, Macro-structuring clathrates to boost the system-level methane storage capacity, *Chem. Eng. J.*, 2025, **519**, 164908.
24 A. A. Bhosle, M. Banerjee and A. Chatterjee, Aggregation-induced emission-active azines for chemosensing applications: A five-year update, *Sens. Diagn.*, 2024, **3**, 745–782.
25 Q. Lin, X. Ding, Y. Hou, W. Ali, Z. Li, X. Han, Z. Meng, Y. Sun and Y. Liu, Adsorption and separation technologies based on supramolecular macrocycles for water treatment, *Eco-Environ. Health*, 2024, **3**, 381–391.
26 K. M. Sahu, S. Patra and S. K. Swain, Host-guest drug delivery by β-cyclodextrin assisted polysaccharide vehicles: A review, *Int. J. Biol. Macromol.*, 2023, **240**, 124338.
27 D. Seebach, A. K. Beck and H. Heckel, TADDOLs, their derivatives, and TADDOL analogues: Versatile chiral auxiliaries, *Angew. Chem., Int. Ed.*, 2001, **40**, 92–138.
28 S. Zhu, P. R. F. Bell and P. F. Greenfield, Adsorption of pyridine onto spent Rundle oil shale in dilute aqueous solution, *Water Res.*, 1988, **22**, 1331–1337.
29 G. B. Daware and P. R. Gogate, Sonochemical degradation of 3-methylpyridine (3MP) intensifies using combination with various oxidants, *Ultrason. Sonochem.*, 2020, **67**, 105120.
30 E. Li, Y. Zhen, L. Chen, X. Li, L. Li, W. Lu, T. Li, Q. Li and Y. Yu, Thermodynamic and quantum chemical investigation of MIBK as a liquid phase extraction solvent for separating pyridine compounds from water, *J. Mol. Liq.*, 2024, **403**, 124876.
31 Bruker, *APEX2, SADABS and SAINT*, Bruker AXS, Madison, 2010.
32 G. M. Sheldrick, SHELXT–Integrated space-group and crystal-structure determination, *Acta Crystallogr., Sect. A: Found. Adv.*, 2015, **71**, 3–8.
33 G. M. Sheldrick, Crystal structure refinement with SHELXL, *Acta Crystallogr., Sect. C: Struct. Chem.*, 2015, **71**, 3–8.
34 C. B. Hübschle, G. M. Sheldrick and B. Dittrich, ShelXle: a Qt graphical user interface for SHELXL, *J. Appl. Crystallogr.*, 2011, **44**, 1281–1284.
35 Bruker, *APEX3 v2019.1–0, SAINT V8.40A*, Bruker AXS Inc., Madison (WI), USA, 2019.
36 L. Krause, R. Herbst-Irmer, G. M. Sheldrick and D. Stalke, Comparison of silver and molybdenum microfocus X-ray sources for single-crystal structure determination, *J. Appl. Crystallogr.*, 2015, **48**, 3–10.
37 G. M. Sheldrick, A short history of SHELX, *Acta Crystallogr., Sect. A: Found. Crystallogr.*, 2008, **64**, 112–122.
38 L. J. Barbour, X-Seed–A software tool for supramolecular crystallography, *J. Supramol. Chem.*, 2001, **1**, 189–191.
39 E. Weber, N. Dörpinghaus and I. Csöregh, Versatile and convenient lattice hosts derived from singly bridged triarylmethane frameworks, X-ray crystal structures of three inclusion compounds, *J. Chem. Soc., Perkin Trans. 2*, 1990, **12**, 2167–2177.
40 B. Taljaard, A. Goosen and C. W. McCleland, Synthesis of hydrogen peroxide: acid-catalysed decomposition of 9-hydroperoxy-9-phenylxanthene and its derivatives, *S. Afr. J. Chem.*, 1987, **40**, 139–145.
41 B. Barnardo, B. Barton, M. R. Caira and E. C. Hosten, Evaluation of the behaviour of two tricyclic-fused host systems in the presence of single and mixed isomers of the C_8H_{10} aromatic crude oil fraction, *Cryst. Growth Des.*, 2024, **24**, 5603–5613.
42 B. Barnardo, B. Barton and E. C. Hosten, The host behaviour of 9-phenyl-9H-xanthene derivatives in mixtures of cyclohexanone and the methylcyclohexanone isomers, *J. Inclusion Phenom. Macrocyclic Chem.*, 2024, **104**, 597–609.
43 B. Barnardo, B. Barton and E. C. Hosten, Alternative separation strategy for o–/p-dichlorobenzene mixtures through supramolecular chemistry protocols, *CrystEngComm*, 2024, **26**, 4876–4885.
44 B. Barnardo, B. Barton, M. R. Caira and E. C. Hosten, Enclathration of saturated five-membered rings by tricyclic fused host systems, *Cryst. Growth Des.*, 2024, **24**, 10326–10337.
45 A. M. Pivovar, K. T. Holman and M. D. Ward, Shape-selective separation of molecular isomers with tunable hydrogen-bonded host frameworks, *Chem. Mater.*, 2001, **13**, 3018–3031.
46 N. M. Sykes, H. Su, E. Weber, S. A. Bourne and L. R. Nassimbeni, Selective enclathration of methyl- and dimethylpiperidines by fluorenol hosts, *Cryst. Growth Des.*, 2016, **17**, 819–826.
47 C. F. Macrae, I. Sovago, S. J. Cottrell, P. T. A. Galek, P. McCabe, E. Pidcock, M. Platings, G. P. Shields, J. S. Stevens, M. Towler and P. A. Wood, Mercury 4.0: from visualization to analysis, design and prediction, *J. Appl. Crystallogr.*, 2020, **53**, 226–235.
48 (*a*) CCDC 2463135: Experimental Crystal Structure Determination, 2025, DOI: 10.5517/ccdc.csd.cc2np2zf; (*b*) CCDC 2463136: Experimental Crystal Structure Determination, 2025, DOI: 10.5517/ccdc.csd.cc2np30h; (*c*) CCDC 2463137: Experimental Crystal Structure Determination, 2025, DOI: 10.5517/ccdc.csd.cc2np31j; (*d*) CCDC 2463139: Experimental Crystal Structure Determination, 2025, DOI: 10.5517/ccdc.csd.cc2np33l; (*e*)

CCDC 2463141: Experimental Crystal Structure Determination, 2025, DOI: 10.5517/ccdc.csd.cc2np35n; (*f*) CCDC 2463337: Experimental Crystal Structure Determination, 2025, DOI: 10.5517/ccdc.csd.cc2np9h5; (*g*) CCDC 2467552: Experimental Crystal Structure Determination, 2025, DOI: 10.5517/ccdc.csd.cc2ntpgn; (*h*) CCDC 2467553: Experimental Crystal Structure Determination, 2025, DOI: 10.5517/ccdc.csd.cc2ntphp.